Volume 27
Number 9
7 March 2025
Pages 1217–1364

CrystEngComm

rsc.li/crystengcomm

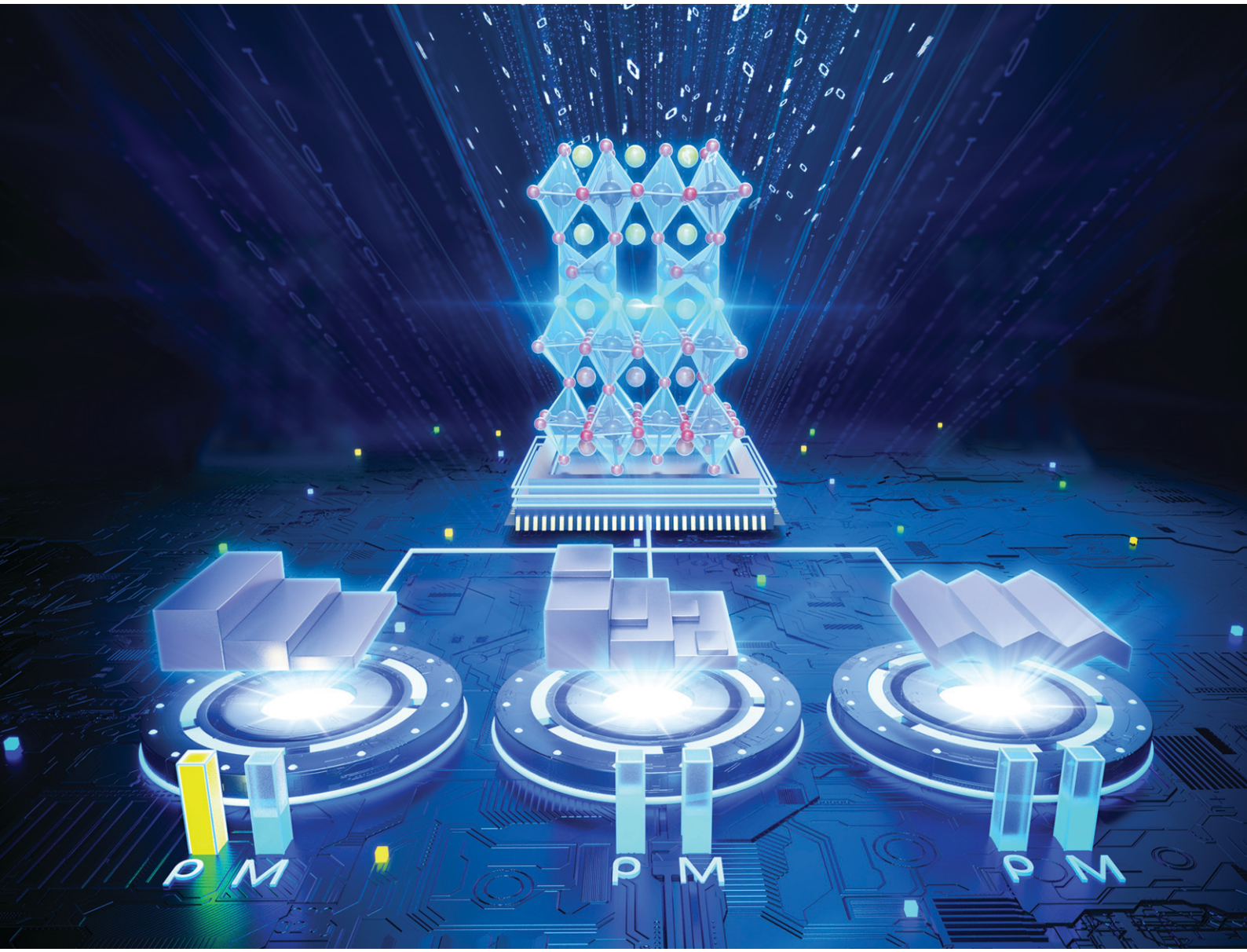

ISSN 1466-8033

ROYAL SOCIETY OF CHEMISTRY

PAPER

Chonglin Chen *et al.*

Substrate-surface-structure tuned electrical and magnetic properties of $PrCoO_3/CaCoO_{2.5}$ superlattices

CrystEngComm

ROYAL SOCIETY OF CHEMISTRY

PAPER

View Article Online
View Journal | View Issue

Cite this: *CrystEngComm*, 2025, **27**, 1256

Substrate-surface-structure tuned electrical and magnetic properties of $PrCoO_3/CaCoO_{2.5}$ superlattices†

Xiaomin Jia,[a] Yanbin Chen,[a] Ce-Wen Nan,[a] Jing Ma*[a] and Chonglin Chen*[b]

Interface engineering using substrate surface structures, especially the surface steps, terraces, and facets, is an effective way of tuning the physical properties of epitaxial films and superstructures. The superlattices comprising perovskite $PrCoO_3$ and brownmillerite $CaCoO_{2.5}$ were grown on three different surface structures, namely, the (001) $SrTiO_3$ substrate with clear surface-step-terraces, the (001) $(LaAlO_3)_{0.3}(Sr_2AlTaO_6)_{0.7}$ (LSAT) substrate with poorly defined surface-step-terraces, and the (001) $LaAlO_3$ substrate with zig-zag surface facets. The superlattices on $LaAlO_3$ substrates not only exhibit superior ferromagnetic properties but also greater electrical conductivity, with their room-temperature resistivities at the most four orders of magnitude smaller than those on $SrTiO_3$ and LSAT substrates. The antiphase domain boundaries that extend all the way from the interface to the surface can be formed at the edges of the surface-step-terraces, which impede the pathways for charge carrier hopping and magnetic exchange interactions, thereby leading to the well-disciplined ferromagnetic insulating properties of the superlattices on $SrTiO_3$ and LSAT substrates. These results provide new insights into the understanding of the correlation between substrate surface structures and physical properties of the superlattice system.

Received 18th November 2024,
Accepted 3rd January 2025

DOI: 10.1039/d4ce01166j

rsc.li/crystengcomm

1. Introduction

Substrate surface structures, *i.e.*, surface terminations and step heights, have received considerable research attention because of their significant impact on the different functionalities of highly epitaxial oxide thin films.[1–8] There are various steps, terraces, and other defects on the crystalline surfaces.[8–12] For instance, on the (001) $SrTiO_3$ (STO) substrate, the TiO_2 termination is more stable than the SrO termination at the deposition temperatures for most transition metal oxides and many surface-step-terraces appear (Fig. 1a).[13–15] Another representative morphology of perovskite substrates is the facetted surfaces on the (001) $LaAlO_3$ (LAO) substrate. The LAO substrate undergoes a ferroelastic phase transition at 544 °C.[16,17] The twinned rhombohedral microstructure at room temperature leads to periodic corrugation with zig-zag facets on the (001) LAO surfaces (Fig. 1b).[18–20] However, the surface structure of the (001) $(LaAlO_3)_{0.3}(Sr_2AlTaO_6)_{0.7}$ (LSAT) substrate lies intermediate between that of the (001) STO and (001) LAO substrates. Although there are no twins in the LSAT substrate, the annealing temperature is required to exceed 1100 °C to achieve clear and defined terraces on the LSAT surfaces. The LSAT surfaces usually exhibit poorly defined steps, terraces, and mounds at the film deposition temperature.[21] Therefore, the epitaxial quality of the oxide thin films is highly dependent upon the substrate surface structures.

The step heights, terrace dimensions, and edge/facet distributions on the substrate surface play a key role in governing the microstructures, including both conservative and non-conservative antiphase domain boundaries (APBs), and the physical properties of the epitaxial films.[2,23] Furthermore, the mismatch between the film unit-cell arrangement and the substrate surface-step-terrace dimensions results in additional strain energy stored in the films, named "residual matching".[24] For example, the electronic transport and magnetic properties of the $LaBaCo_2O_{5.5+\delta}$ films can be strongly regulated by the dimension of surface terraces,[13,25,26] and the superconducting properties of the $YBa_2Cu_3O_{7-\delta}$ films are highly dependent on the surface facets of the twinned substrate.[27,28] Recently, we found that the substrate surface structures are crucial not only for the single-layer cobaltate films but also for their superlattices (SLs).[22] Specifically, the APBs and electronic transport properties of the SLs comprising perovskite $PrCoO_3$ (PCO) and brownmillerite $CaCoO_{2.5}$ (CCO) have extraordinary sensitivity to the surface-step-terraces on the (001) STO substrate. However, most research studies on substrate surface

[a] *School of Materials Science and Engineering, Tsinghua University, Beijing 100084, China. E-mail: ma-jing@mail.tsinghua.edu.cn*
[b] *Department of Physics and Astronomy & Advanced Materials Engineering Program, University of Texas at San Antonio, San Antonio, Texas 78249, USA. E-mail: chonglin.chen@utsa.edu*

† Electronic supplementary information (ESI) available. See DOI: https://doi.org/10.1039/d4ce01166j

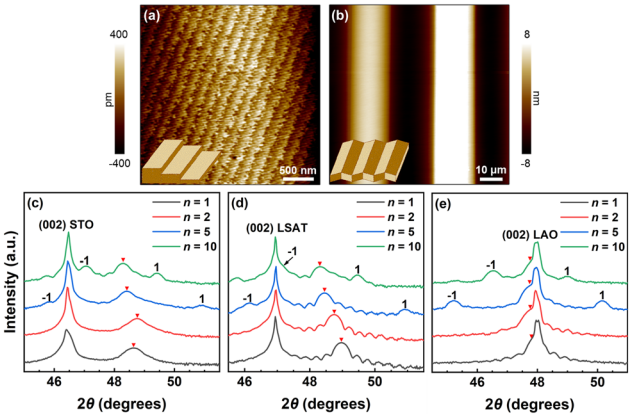

Fig. 1 (a) and (b) Typical atomic force microscopy images of commercially available perovskite substrates with surface-step-terraces [(001) STO substrate] and surface facets [(001) LAO substrate], respectively. The insets show a schematic drawing of the surface morphology of these substrates. (c)–(e) X-ray diffraction θ–2θ patterns of the as-grown SLs around the (002) peaks of the substrates. The main (002) peaks and satellite peaks of the SLs are indicated by red triangles and numbers, respectively. For easy comparison, (c) is replotted from ref. 22.

structures focus on single-layer oxide films, and no systematic study has been conducted to investigate the effects of various substrate surface structures on oxide SLs.

To systematically investigate the substrate effects on the physical properties of highly epitaxial films and heterostructures, we extended the SLs composed of perovskite PCO and brownmillerite CCO on the (001) STO substrates with a well-defined surface-step-terrace structure to other substrates, *i.e.*, the (001) LSAT substrates with an unwell-defined surface-step-terrace structure, and the (001) LAO substrates with a twinned zig-zag facet structure. Our results indicate that the room-temperature resistivity of the SLs on STO and LSAT substrates is at the most four orders of magnitude larger than that on LAO substrates. While the saturation magnetization on LAO substrates is greater than that on the other two substrates, which is nearly twice that on LSAT substrates. The enhanced insulating and reduced ferromagnetic properties on STO and LSAT substrates can be attributed to the APBs that formed at the edges of terraces continuing throughout the SLs, which induce additional scattering of charge carriers and break the paths of the magnetic exchange interactions across the APBs. These findings enable one to design and explore new emergent phenomena in multifunctional oxide SLs by the surface engineering technique.

2. Results and discussion

The $[(PCO)_n/(CCO)_n]_m$ SLs, simplified as $(PCO)_n/(CCO)_n$ SLs (n = 1, 2, 5, and 10, denotes the number of unit cells in a period; m = 40, 20, 8, and 4, respectively, denotes the number of periods in a SL) with a total thickness of 32 nm were fabricated by pulsed laser deposition (PLD). Details of the epitaxial growth of SLs are given in the ESI.† The X-ray diffraction (XRD) patterns of the PCO/CCO bilayer films are shown in Fig. S1.† The half-order (0 0 1/2) peaks in the XRD spectra indicate the brownmillerite structure of the CCO films. Fig. 1c–e show the XRD θ–2θ scans of the $(PCO)_n/(CCO)_n$ SLs around the (002) peaks of the substrates. The satellite peaks of the n = 1 and n = 2 SLs exhibit a very low diffraction intensity and are located at considerable angular distances from the main peaks due to their small period thicknesses, as seen in Fig. S2.† The calculated period thicknesses of all the SLs from the angle distance between adjacent satellite peaks are summarized in Fig. S3,† which align well with the designed period thicknesses, indicating precise control over the growth of the SLs. The reciprocal space mapping (RSM) of the (103) reflection shows that these SLs are fully strained by the LSAT and LAO substrates, but can partially relieve the strain when grown on STO substrates, as seen in Fig. S4.†

We then measured the electrical transport properties of the $(PCO)_n/(CCO)_n$ SLs. Fig. 2a–c show the temperature dependence of the resistivity of the SLs on different substrates and the room-temperature resistivities in the insets. Obviously, the resistivity is highly dependent upon the type of the substrate, especially for the short-period SLs with n = 1 and 2. For the SLs on STO and LSAT substrates with surface-step-terraces, the resistivity generally decreases as n is reduced from 10 to 2, with the exception of a slight increase for the n = 2 SL near room temperature, as seen in the insets of Fig. 2a and b. The SL with n = 1 has a significantly larger resistivity than other samples, with its room-temperature resistivity about three orders of magnitude larger than that of the n = 5 SL. Furthermore, the resistivity of the n = 1 SL on the STO substrate is nearly twice

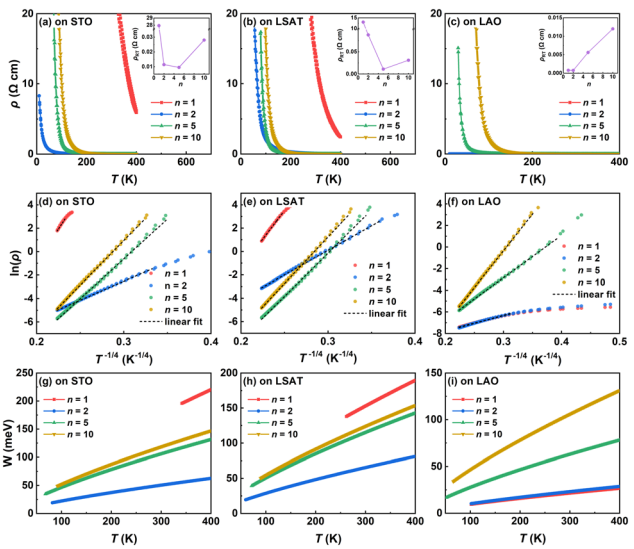

Fig. 2 Electrical transport characteristics of the $(PCO)_n/(CCO)_n$ SLs. (a)–(c) Temperature-dependent resistivity of the SLs on the (001) STO, (001) LSAT, and (001) LAO substrates, respectively. The insets show the variation of the room-temperature (RT) resistivity with n. (d)–(f) Fitting the resistivity data using Mott's variable range hopping (VRH) model ($\ln \rho \propto T^{-1/4}$). (g)–(i) The hopping energy as a function of temperature. For easy comparison, (a) is replotted from ref. 22.

that on the LSAT substrate despite the presence of steps and terraces on the surfaces of both substrates. In contrast, for the SLs deposited on LAO substrates with surface facets, the resistivity monotonically decreases with decreasing n over the entire range of measured temperatures, as shown in Fig. 2c. The room-temperature resistivity of the n = 1 SL on LAO substrates is four orders of magnitude smaller than that on STO and LSAT substrates.

To elucidate the origin of the distinct electrical transport characteristics on different substrates, we first employed X-ray photoelectron spectroscopy (XPS) measurements to analyze the atomic states of these SLs. Fig. S5† shows the Co 2p core peaks of the SLs on various substrates. A mixed Co valence state of +3 and +4 is found in all the SLs on these three substrates, and the Co^{4+}/Co^{3+} ratio increases with decreasing n, as seen in Fig. S5d.† Since the Co ions in stoichiometric bulk PCO and CCO exhibit a valence state of +3, the increase in the nominal valence state of Co ions implies a reduction in the oxygen vacancy concentration within the SL system to maintain charge conservation. The variation of oxygen stoichiometry may originate from the PCO/CCO interfaces, where the oxygen vacancy formation in the tetrahedral sub-layers of the brownmillerite CCO on one side of the interface would be suppressed by adjacent octahedral sub-layers of the perovskite PCO on the other side to maintain the continuity of the interfacial structure, and this suppression effect is greatly magnified in short-period SLs.[29] Therefore, we observed a continuous rise in the valence state of Co ions as the interfacial density increases (or n decreases). Then, the increased conductivity with decreased n for the SLs on LAO substrates and for the longer-period SLs (n = 2, 5, and 10) on STO and LSAT substrates can be ascribed to the enhanced charge carrier hopping from Co^{3+} to Co^{4+}.

The significantly large resistivity of the short-period SLs on STO substrates is closely related to the APBs formed at the edges of surface terraces, which we have extensively studied in our previous research.[22] The (001) STO substrates are commonly treated with cutting and polishing, and exhibit a mixed termination of SrO and TiO_2 (Fig. 3b). However, the TiO_2 termination is more stable than the SrO termination after thermal treatment. Therefore, the (001) STO substrates show the TiO_2 surface termination and consist of many surface-step-terraces with each step height of one unit cell before growing the SLs (Fig. 3c).[13] For the n = 1 SL, the thickness of each constituent layer is ~0.4 nm, which is close to the step height on the (001) STO surfaces. With continuous layer-by-layer growth, perpendicular APBs would be formed at the edges of surface terraces and penetrate the entire SL thickness (Fig. S6†). These APBs act as additional scattering centers of charge carriers and reduce the mobility of charge carriers across the step edges, leading to the good insulating behavior of the n = 1 SL. For the n = 2 SL, the thickness of each PCO and CCO layer is ~0.8 nm, which is twice the step height of the (001) STO surface. Only a small number of discontinuous APBs can be formed in the SLs (see Fig. S6†),

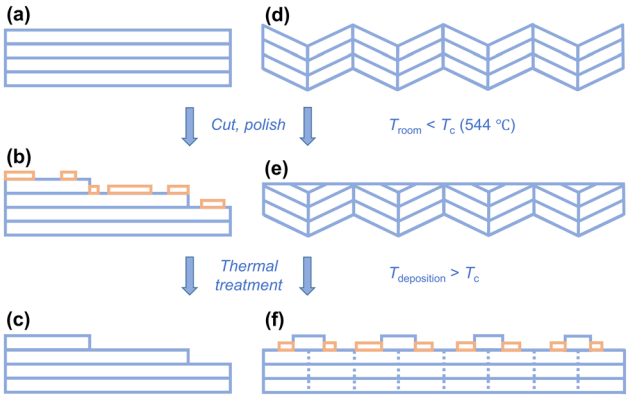

Fig. 3 The evolution of different substrate surface structures. (a)–(c) The surface-step-terrace structure on the STO substrate. (d)–(f) The twinned zig-zag facet structure on the LAO substrate. T_c is the phase transition temperature (544 °C) of LAO from the pseudocubic rhombohedral $R\bar{3}c$ phase to the cubic $Pm3m$ phase.

providing pathways for charge carriers traversing across the step edges. Therefore, its resistivity is significantly lower than that of the n = 1 SL. For the SLs with $n \geq 5$, the thickness of each PCO and CCO layer is much larger, so the carrier scattering effect induced by the APBs becomes negligible.

The (001) LSAT substrates also show a surface-step-terrace morphology, but the steps and terraces are poorly defined compared to those on STO surfaces since they require a temperature exceeding 1100 °C to achieve clear and defined step-terrace structures.[30] This implies that the shape of the surface-step-terrace edges on the LSAT substrate deviates from straightness and becomes irregular at the deposition temperature. Furthermore, the LSAT surfaces show mixed A-site and B-site terminations with the step height not confined to one unit cell,[21] leading to fewer APBs formed on the LSAT surfaces. The less APB structures will result in less carrier scattering at the boundaries in the n = 1 SL. Therefore, the resistivity of the n = 1 SL on the LSAT substrate is almost half of that on the STO substrate. Unlike the (001) STO and (001) LSAT surfaces, the (001) LAO surface always consists of zig-zag surface facets due to its twinned rhombohedral microstructure at the temperature below 544 °C (Fig. 3d).[11] After cutting and polishing, the LAO substrate can show a macroscopic (001) surface (Fig. 3e). It is important to know that on the (001) LAO substrate, the surface termination is mainly a LaO top layer after annealing at ~850 °C but becomes an AlO_2 top layer for annealing at a temperature higher than 900 °C.[11] Since the film was deposited at the temperature of 750 °C, higher than the phase transition temperature (544 °C) of LAO from the pseudocubic rhombohedral $R\bar{3}c$ phase to the cubic $Pm3m$ phase,[11] the wedge-shaped morphology should have reappeared in the substrate by the partial reconstruction of the surface steps, terraces, and kinks, as seen in Fig. 3f. Therefore, the penetrating APBs that resulted from the step-and-terrace structure on STO and LSAT substrates are absent in the SLs on LAO substrates, leading to their higher conductivity.

To determine the mechanism of the transport behavior, the temperature-dependent resistivity data were fit to different models.[31–33] We found that Mott's variable range hopping (VRH) model best fits the data near room temperature, as shown in Fig. 2d–f. The VRH model is usually used in various disordered systems where charge carriers move by hopping between localized electronic states.[34] As discussed earlier, the Co^{4+} ions in the SLs originated from the variation of oxygen stoichiometry at the PCO/CCO interfaces. Therefore, the charge transfer between Co^{4+} and Co^{3+} ions is mainly localized in small regions near the interfaces. The electrical transport of these SLs is then dominated by hopping in the conduction channels at a single interface or between conduction channels at different interfaces when the distance between adjacent interfaces is very small, such as in some short-period SLs.[35,36] We estimated the hopping energy (W) based on the slope of the fitted curves.[37] Fig. 2g–i show the hopping energy as a function of temperature. For the SLs on LAO substrates, the hopping energy decreases monotonically with decreasing n due to the increasing interfacial density and thus interfacial charge transfer regions. While for the SLs on STO and LSAT substrates, the hopping energy of the n = 1 SL is substantially enhanced, possessing the highest value among all samples. This is due to the fact that the charge carriers have to overcome the APBs to hop from one domain to another in the n = 1 SL, resulting in their increased hopping difficulty. Furthermore, the n = 1 SL on the STO substrate has a larger hopping energy than that on the LSAT substrate since vertically penetrating APBs are more readily formed on the STO surfaces with clear steps and terraces.

Apart from the electrical transport properties, the substrate surface structures can also strongly modulate the magnetic properties of the SLs, as seen in Fig. 4. For comparison, the magnetic hysteresis loops of the cation-disordered $Pr_{0.5}Ca_{0.5}CoO_{3-\delta}$ (PCCO) films are also displayed. We found that the hysteresis loop of the PCCO film on the LAO substrate is a combination of two loops, which should be attributed to the nanoscale-ordered and disordered PCCO phases in the film.[26] The nanoscale-ordered phase is dominant in the film with small strain, whereas the disordered phase is dominant with large strain.[2] The smaller lattice mismatch between PCCO and LAO (+0.41%)[38] may lead to more nanoscale-ordered phases in the film on the LAO substrate and thus its double-loop structure. All the SLs exhibit ferromagnetism, with short-period SLs possessing larger saturation magnetization. The ratio of Co^{4+}/Co^{3+} shows a rise with the decrease of n (Fig. S5†), so the magnetic exchange interactions between Co^{3+} and Co^{4+} may account for the emergence of ferromagnetism in the SLs.

The n = 1 SL can be regarded as a cation-ordered PCCO film where the Pr^{3+} and Ca^{2+} ions are separated by the interfaces of the SLs. Considering the promoting effect of cation ordering on magnetic exchange interactions,[39,40] the n = 1 SL is expected to exhibit stronger magnetism than the disordered PCCO films. The n = 1 SL on the LAO substrate indeed has larger magnetization than the PCCO films, but on STO and LSAT substrates has remarkably smaller magnetization. Moreover, the n = 1 SL on the LAO substrate demonstrates notably superior magnetic properties than that on other substrates, with its saturation magnetization being approximately twice that on the LSAT substrate. These phenomena are probably related to the substrate-induced strain and the defects in the SLs. On the one hand, the compressive strain from the LAO substrate (see Fig. 1 and S4†) could induce the shortening of the Co–O–Co bond length, making the magnetic exchange easier and increasing the magnetic moment, which is also found in our previous studies.[26] On the other hand, the SLs on STO and LSAT substrates have greater strain than those on LAO substrates, which may lead to the formation of more lattice defects, such as dislocations, to relieve the strain energy. Furthermore, the APBs can nucleate at the edges of the steps on STO and LSAT surfaces. Therefore, the probability of spin scattering can be greatly increased owing to the obstacles from APBs, dislocations, and other defects in the SLs, resulting in the weakening of magnetism.[41] Nevertheless, the SLs on various substrates demonstrate magnetic moments of the same magnitude though their resistivities differ by orders of magnitude, exhibiting a great potential for tunable ferromagnetic insulators.

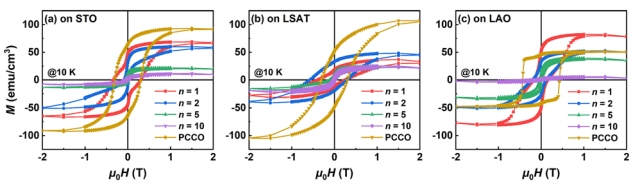

Fig. 4 Magnetic-field dependence of the magnetization curves of the $(PCO)_n/(CCO)_n$ SLs and PCCO films measured at 10 K on the (a) (001) STO, (b) (001) LSAT, and (c) (001) LAO substrates, respectively. For easy comparison, (a) is replotted from ref. 22.

3. Conclusions

In summary, epitaxial $(PCO)_n/(CCO)_n$ SLs were epitaxially grown on (001) STO, (001) LSAT, and (001) LAO substrates to systematically investigate the effect of substrate surface structures on the electronic transport and magnetic properties. The APBs were formed at the edges of the surface-step-terraces on STO and LSAT substrates, which impede the migration of charge carriers from one domain to another and disrupt the magnetic exchange pathways, leading to increased resistivity and diminished ferromagnetism of the SLs. The room-temperature resistivity of the n = 1 SL on the LAO substrate is four orders of magnitude smaller than that on the other two substrates, while its saturation magnetization is at the most twice that on the other two substrates. The greater modulation capability of the substrate surface structures on insulating properties than on magnetic properties paves a new way for designing and fabricating artificial materials with excellent ferromagnetic insulating properties.

Data availability

The data that support the findings of this study are available in the ESI† of this article.

Conflicts of interest

There are no conflicts to declare.

Acknowledgements

This work was supported by the National Natural Science Foundation of China (Grant No. 52421001, 52388201, and 52027817).

Notes and references

1 Y. Lin and C. Chen, Interface effects on highly epitaxial ferroelectric thin films, *J. Mater. Sci.*, 2009, **44**, 5274–5287.
2 C. Ma, M. Liu, J. Liu, G. Collins, Y. Zhang, H. Wang, C. Chen, Y. Lin, J. He, J. Jiang, E. I. Meletis and A. J. Jacobson, Interface effects on the electronic transport properties in highly epitaxial $LaBaCo_2O_{5.5+\delta}$ films, *ACS Appl. Mater. Interfaces*, 2014, **6**, 2540–2545.
3 F. Sanchez, C. Ocal and J. Fontcuberta, Tailored surfaces of perovskite oxide substrates for conducted growth of thin films, *Chem. Soc. Rev.*, 2014, **43**, 2272–2285.
4 X. N. Zhu, T. T. Gao, X. Xu, W. Z. Liang, Y. Lin, C. Chen and X. M. Chen, Piezoelectric and dielectric properties of multilayered $BaTiO_3$/(Ba,Ca)TiO_3/$CaTiO_3$ thin films, *ACS Appl. Mater. Interfaces*, 2016, **8**, 22309–22315.
5 A. Biswas, C.-H. Yang, R. Ramesh and Y. H. Jeong, Atomically flat single terminated oxide substrate surfaces, *Prog. Surf. Sci.*, 2017, **92**, 117–141.
6 Y. Yang, L. Wang, H. Huang, C. Kang, H. Zong, C. Zou, Y. Lu, X. Li, B. Hong and C. Gao, Controlling metal-insulator transition in (010)-VO_2/(0001)-Al_2O_3 epitaxial thin film through surface morphological engineering, *Ceram. Int.*, 2018, **44**, 3348–3355.
7 H. Wang, Z. Wang, Z. Ali, E. Wang, M. Saghayezhian, J. Guo, Y. Zhu, J. Tao and J. Zhang, Surface termination effect of $SrTiO_3$ substrate on ultrathin $SrRuO_3$, *Phys. Rev. Mater.*, 2024, **8**, 013605.
8 C. Chen and T. T. Tsong, Behavior of Ir atoms and clusters on Ir surfaces, *Phys. Rev. B*, 1990, **41**, 12403–12412.
9 Y. J. Chang and S.-h. Phark, Atomic-scale visualization of initial growth of perovskites on $SrTiO_3$ (001) using scanning tunneling microscope, *Curr. Appl. Phys.*, 2017, **17**, 640–656.
10 C. L. Chen, Y. Cao, Z. J. Huang, Q. D. Jiang, Z. Zhang, Y. Y. Sun, W. N. Kang, L. M. Dezaneti, W. K. Chu and C. W. Chu, Epitaxial $SrRuO_3$ thin films on (001) $SrTiO_3$, *Appl. Phys. Lett.*, 1997, **71**, 1047–1049.
11 H.-J. Gao, C. L. Chen, B. Rafferty, S. J. Pennycook, G. P. Luo and C. W. Chu, Atomic structure of $Ba_{0.5}Sr_{0.5}TiO_3$ thin films on $LaAlO_3$, *Appl. Phys. Lett.*, 1999, **75**, 2542–2544.
12 J. H. Chen, C. L. Lia, K. Urban and C. L. Chen, Unusual lattice distortion in a $Ba_{0.5}Sr_{0.5}TiO_3$ thin film on a $LaAlO_3$ substrate, *Appl. Phys. Lett.*, 2002, **81**, 1291–1293.
13 Q. Zou, M. Liu, G. Wang, H. Lu, T. Yang, H. Guo, C. Ma, X. Xu, M. Zhang, J. Jiang, E. I. Meletis, Y. Lin, H. Gao and C. Chen, Step terrace tuned anisotropic transport properties of highly epitaxial $LaBaCo_2O_{5.5+\delta}$ thin films on vicinal $SrTiO_3$ substrates, *ACS Appl. Mater. Interfaces*, 2014, **6**, 6704–6708.
14 R. Eason, *Pulsed laser deposition of thin films: applications-led growth of functional materials*, John Wiley & Sons Ltd., Hoboken, USA & Chichester, UK, 2006.
15 G.-B. Cho, M. Yamamoto and Y. Endo, Surface features of self-organized $SrTiO_3$ (001) substrates inclined in [100] and [110] directions, *Thin Solid Films*, 2004, **464–465**, 80–84.
16 Z. Hussain, D. Kumar and V. R. Reddy, Effect of ferro-elastic twin domains of $LaAlO_3$ substrate on the magnetic anisotropy and the magnetization reversal process of cobalt thin film, *J. Magn. Magn. Mater.*, 2019, **477**, 408–414.
17 S. Bueble, K. Knorr, E. Brecht and W. W. Schmahl, Influence of the ferroelastic twin domain structure on the {100} surface morphology of $LaAlO_3$ HTSC substrates, *Surf. Sci.*, 1998, **400**, 345–355.
18 C. Li, Y. Zhang, Q. Ji, J. Shi, Z. Chen, X. Zhou, Q. Fang and Y. Zhang, Substrate effect on the growth of monolayer dendritic MoS_2 on $LaAlO_3$ (100) and its electrocatalytic applications, *2D Mater.*, 2016, **3**, 035001.
19 O. I. Lebedev, G. V. Tendeloo, S. Amelinckx, H. L. Ju and K. M. Krishnan, High-resolution electron microscopy study of strained epitaxial $La_{0.7}Sr_{0.3}MnO_3$ thin films, *Philos. Mag. A*, 2000, **80**, 673–691.
20 A. A. Burema, J. J. L. van Rijn and T. Banerjee, Temperature dependence of the magnetization of $La_{0.67}Sr_{0.33}MnO_3$ thin films on $LaAlO_3$, *J. Vac. Sci. Technol., A*, 2019, **37**, 021103.
21 J. H. Ngai, T. C. Schwendemann, A. E. Walker, Y. Segal, F. J. Walker, E. I. Altman and C. H. Ahn, Achieving A-site termination on $La_{0.18}Sr_{0.82}Al_{0.59}Ta_{0.41}O_3$ substrates, *Adv. Mater.*, 2010, **22**, 2945–2948.
22 X. Jia, Y. Chen, C.-W. Nan, J. Ma and C. Chen, Engineering antiphase domain boundaries boosted tunable ferromagnetic insulation, *Appl. Phys. Lett.*, 2024, **125**, 151605.
23 J. Jiang, Y. Lin, C. Chen, C. Chu and E. Meletis, Microstructures and surface step-induced antiphase boundaries in epitaxial ferroelectric $Ba_{0.6}Sr_{0.4}TiO_3$ thin film on MgO, *J. Appl. Phys.*, 2002, **91**, 3188–3192.
24 C. Ma, M. Liu, C. Chen, Y. Lin, Y. Li, J. S. Horwitz, J. Jiang, E. I. Meletis and Q. Zhang, The origin of local strain in highly epitaxial oxide thin films, *Sci. Rep.*, 2013, **3**, 3092.
25 C. Ma, M. Liu, G. Collins, H. Wang, S. Bao, X. Xu, E. Enriquez, C. Chen, Y. Lin and M.-H. Whangbo, Magnetic and electrical transport properties of $LaBaCo_2O_{5.5+\delta}$ thin films on vicinal (001) $SrTiO_3$ surfaces, *ACS Appl. Mater. Interfaces*, 2013, **5**, 451–455.
26 M. Liu, S. Ren, J. Lu, C. Ma, X. Xu and C. Chen, Surface-step-terrace tuned magnetic properties of epitaxial $LaBaCo_2O_{5.5+\delta}$ thin films on vicinal (La,Sr)(Al,Ta)O_3 substrates, *CrystEngComm*, 2015, **17**, 8339–8344.

27 Z.-X. Ye, Q. Li, Y. Hu, W. Si, P. Johnson and Y. Zhu, Enhanced flux pinning in $YBa_2Cu_3O_{7-\delta}$ films by nanoscaled substrate surface roughness, *Appl. Phys. Lett.*, 2005, **87**, 122502.

28 Y. Zuxin, L. Qiang, W. D. Si and P. D. Johnson, Critical current density enhancement in $YBa_2Cu_3O_{7-\delta}$ thin films by twin domains of $LaAlO_3$ substrates, *IEEE Trans. Appl. Supercond.*, 2005, **15**, 3013–3015.

29 S. Cook, T. K. Andersen, H. Hong, R. A. Rosenberg, L. D. Marks and D. D. Fong, Engineering the oxygen coordination in digital superlattices, *APL Mater.*, 2017, **5**, 126101.

30 P. Pranav Pradeep, P. C. Shyni, V. Gopal, S. G. Bhat and P. S. A. Kumar, LSAT (001) termination: an investigation on the influence of annealing parameters on topography, *Phys. B*, 2022, **640**, 414092.

31 T. T. M. Palstra, B. Batlogg, L. F. Schneemeyer and J. V. Waszczak, Thermally activated dissipation in $Bi_{2.2}Sr_2Ca_{0.8}Cu_2O_{8+\delta}$, *Phys. Rev. Lett.*, 1988, **61**, 1662–1665.

32 A. L. Efros and B. I. Shklovskii, Coulomb gap and low temperature conductivity of disordered systems, *J. Phys. C: Solid State Phys.*, 1975, **8**, L49.

33 N. F. Mott, Conduction in glasses containing transition metal ions, *J. Non-Cryst. Solids*, 1968, **1**, 1–17.

34 S. Bao, S. Pang, W. Wang, J. Chen, M. Chen, J. Ma, C.-W. Nan and C. Chen, Ca doping effect on the magnetic and electronic transport properties in double perovskite $PrBaCo_2O_{5+\delta}$ films, *Appl. Phys. Lett.*, 2017, **111**, 232406.

35 A. Bhattacharya, S. J. May, S. G. te Velthuis, M. Warusawithana, X. Zhai, B. Jiang, J. M. Zuo, M. R. Fitzsimmons, S. D. Bader and J. N. Eckstein, Metal-insulator transition and its relation to magnetic structure in $(LaMnO_3)_{2n}/(SrMnO_3)_n$ superlattices, *Phys. Rev. Lett.*, 2008, **100**, 257203.

36 G. Wang, R. Du, D. Wu and A. Li, Magnetic and transport characteristics of long-period $[(LaMnO_3)_n/(SrMnO_3)_n]_m$ ($n \geq 3$) superlattices, *J. Appl. Phys.*, 2012, **112**, 103917.

37 J. Kurian and R. Singh, Electron spin resonance and resistivity studies of charge-ordered $Bi_{(1-x)}Sr_xMnO_3$, *J. Alloys Compd.*, 2011, **509**, 5127–5136.

38 S. Tsubouchi, T. Kyômen, M. Itoh, P. Ganguly, M. Oguni, Y. Shimojo, Y. Morii and Y. Ishii, Simultaneous metal-insulator and spin-state transitions in $Pr_{0.5}Ca_{0.5}CoO_3$, *Phys. Rev. B*, 2002, **66**, 052418.

39 S. J. May, P. J. Ryan, J. L. Robertson, J. W. Kim, T. S. Santos, E. Karapetrova, J. L. Zarestky, X. Zhai, S. G. te Velthuis, J. N. Eckstein, S. D. Bader and A. Bhattacharya, Enhanced ordering temperatures in antiferromagnetic manganite superlattices, *Nat. Mater.*, 2009, **8**, 892–897.

40 S. Noh, G. Ahn, J. Seo, Z. Gai, H. N. Lee, W. S. Choi and S. J. Moon, $(LaCoO_3)_n/(SrCoO_{2.5})_n$ superlattices: tunable ferromagnetic insulator, *Phys. Rev. B*, 2019, **100**, 064415.

41 J. Wu, R. Guzman, Y. Zhang, H. Chen, Y. Chen, S. Bao, D. Yi, C.-W. Nan, W. Zhou, C. Chen and J. Ma, Lateral magnetic anisotropy modulated by antiphase domain boundaries in $PrBaCo_2O_{5+\delta}$ thin films, *Acta Mater.*, 2023, **247**, 118760.